JOC*Article*

Time-Resolved Resonance Raman Identification and Structural Characterization of a Light Absorbing Transient Intermediate in the Photoinduced Reaction of Benzophenone in 2-Propanol

Yong Du, Chensheng Ma, Wai Ming Kwok, Jiadan Xue, and David Lee Phillips*

Department of Chemistry, The University of Hong Kong, Pokfulam Road, Hong Kong, People's Republic of China

phillips@hkucc.hku.hk

Received May 8, 2007

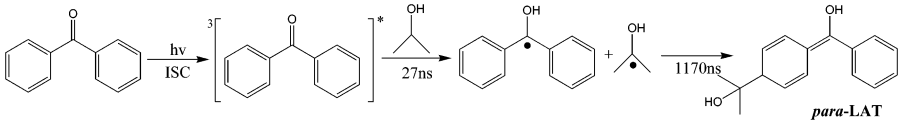

A nanosecond time-resolved resonance Raman (ns-TR^3) spectroscopic study of the triplet state benzophenone reaction with the 2-propanol hydrogen-donor solvent and subsequent reactions is presented. The TR^3 spectra show that the benzophenone triplet state (nπ*) hydrogen-abstraction reaction with 2-propanol is very fast (about 10 to 20 ns) and forms a diphenylketyl radical and an associated 2-propanol radical partner. The temporal evolution of the TR^3 spectra also indicates that recombination of these two radical species occurs with a time constant of about 1170 ns to produce a LAT (light absorbing transient) intermediate that is identified as the 2-[4-(hydroxylphenylmethylene)cyclohexa-2,5-dienyl]propan-2-ol (*p*-LAT) species. Comparison of the TR^3 spectra with results obtained from density functional theory calculations for the species of interest was used to elucidate the identity, structure, properties, and major spectral features of the intermediates observed in the TR^3 spectra. The structures and properties of the reaction intermediates observed (triplet benzophenone, diphenyl ketyl radical, and *p*-LAT) are briefly discussed.

Introduction

Benzophenone (BP) is a prototypical aromatic carbonyl compound that has been extensively studied to better understand its photophysics and photochemistry.[1−9] The photoreduction of benzophenone has received particular interest over the years.[1,2,8] Although Hammond and co-workers[2] worked out the basic mechanism of the photoreduction of benzophenone more than 40 years ago, there has been continuing interest in discerning more details and to develop a deeper understanding of this benchmark photochemistry with advances in technology and spectroscopic methods.[3−9] The lowest excited singlet (S_1 nπ*) and triplet (T_2 $\pi\pi$*) states have a small energy gap and are strongly coupled via a spin−orbit interaction.[6] This small energy gap and strong spin−orbit coupling enables the intersystem crossing (ISC) process to effectively compete kinetically with other S_1 state processes like internal conversion (IC) and fluorescence emission so that the T_1 state is produced with a large yield close to unity.[1−6] Therefore, the major relaxation pathway of the solution-phase photoexcited benzophenone

* Author to whom correspondence should be addressed. Phone: 852-2859-2160. Fax: 852-2857-1586.

(1) Turro, N. J. *Modern Molecular Photochemistry*; University Science Books: Mill Valley, CA, 1991.

(2) Moore, W. M.; Hammond, G. S.; Foss, R. P. *J. Am. Chem. Soc.* **1961**, *83*, 2789−2794.

(3) El-Sayed, M. A. *J. Chem. Phys.* **1963**, *38*, 2834−2838.

(4) (a) Godfrey, T. S.; Hilpern, J. W.; Porter, G. *Chem. Phys. Lett.* **1967**, *1*, 490−492. (b) Rentzepis, P. M. *Science* **1970**, *169*, 239−247. (c) Hochstrasser, R. M.; Wessel, J. E. *Chem. Phys. Lett.* **1973**, *19*, 156−161. (d) Anderson, R. W., Jr.; Hochstrasser, R. M.; Lutz, H.; Scott, G. W. *J. Chem. Phys.* **1974**, *61*, 2500−2506. (e) Hochstrasser, R. M.; Lutz, H.; Scott, G. W. *Chem. Phys. Lett.* **1974**, *24*, 162−167. (f) Hochstrasser, R. M.; Lutz, H.; Scott, G. W. *Chem. Phys. Lett.* **1974**, *28*, 153−157. (g) Topp, M. R. *Chem. Phys. Lett.* **1975**, *32*, 144−149. (h) Bensasson, R. V. *J. Chem. Soc., Faraday I* **1980**, *76*, 1801−1810. (i) Peters, K. S.; Freilich, S. C.; Schaeffer, C. G. *J. Am. Chem. Soc.* **1980**, *102*, 5701−5702. (j) Wagner, P. J.; Truman, R. J.; Scaiano, J. C. *J. Am. Chem. Soc.* **1985**, *107*, 7093−7097. (k) Ohzeki, T.; Ohgus, H.; Isaka, H.; Suzuki, S.; Takahashi, T. *Chem. Phys. Lett.* **1988**, *149*, 379−383. (l) McGarry, P. F.; Doubleday, C. E., Jr.; Wu, C.; Staab, H. A.; Turro, N. J. *J. Photochem. Photobiol. A* **1994**, *77*, 109−117. (m) Bhasikuttan, A. C.; Singh, A. K.; Palit, D. K.; Sapre, A. V.; Mittal, J. P. *J. Phys. Chem. A* **1998**, *102*, 3470−3480. (n) Prater, K.; Freund, W. L.; Bowman, R. M. *Chem. Phys. Lett.* **1998**, *295*, 82−88. (o) Cai, X.; Sakamoto, M.; Hara, M.; Sugimoto, A.; Tojo, S.; Kawai, K.; Endo, M.; Fujitsuka, M.; Majita, T. *Photochem. Photobiol. Sci.* **2003**, *2*, 1209−1214. (p) Okustu, T.; Muramatsu, H.; Horiuchi, H.; Hiratsuka, H. *Chem. Phys. Lett.* **2005**, *404*, 300−303.

10.1021/jo070958d CCC: $37.00
Published on Web 08/23/2007

molecule to the ground state takes place via the T_1 state. The T_1 state is also typically responsible for all of the major photochemical reactions of BP in the solution phase.

The T_1 state of BP has nπ^* character with excitation localized on the carbonyl group in most types of solvents (e.g., most nonpolar, polar, and hydrogen bonding solvents).[1−6,9] Hamaguchi and co-workers reported the observation and analysis of the transient resonance Raman spectra of the T_1 state of BP.[9] They found that the nπ^* triplet state is efficiently photoreduced by hydrogen atom donors and the photolysis of BP in H-donor organic solvents such as isopropyl alcohol (also known as 2-propanol) would result in hydrogen abstraction from the solvent by the ketone to produce a diphenylketyl (DPK) radical[9] consistent with a range of previous photochemical studies.[1−6] The DPK radical and species produced from the H-donor solvent appear to react to produce an intermediate(s) called light absorbing transients (LAT).[8] A variety of experimental methods such as transient absorption spectroscopy have been used to study the LAT species.[8] A number of different species such as an adduct between the ground state BP and the DPK radical, charge-transfer complexes between free radicals, or coupling complexes between different radicals have been proposed for the identity of the LAT species.[8] Attempts to structurally characterize the LAT species by NMR spectroscopy were not successful.[8f] Clear characterization of the LAT species kinetics and other properties by methods like transient absorption spectroscopy are hampered by the overlapping of the n$-\pi^*$ and $\pi-\pi^*$ absorption bands of BP with the LAT absorption and inner filter effects.[8] We note that it appears the LAT species have not yet been characterized by a time-resolved vibrational spectroscopic technique such as time-resolved resonance Raman (TR^3) spectroscopy that can be used to unambiguously identify the LAT species and learn more about its structural and electronic properties. In addition, we also note that the selectivity of TR^3 spectroscopy combined with employment of several probe wavelengths can be very useful to sort out the kinetics of reactions occurring on similar time scales.

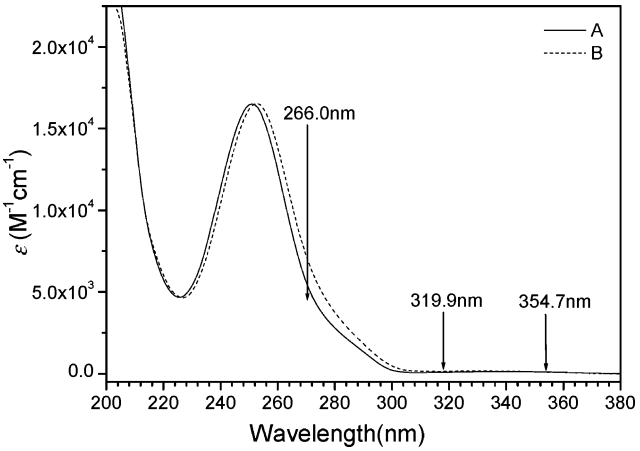

FIGURE 1. Absorption spectra of BP in pure MeCN (A) and 2-propanol (B). The 266 nm pump and 319.9 and 354.7 nm probe wavelengths used in the TR^3 measurements are indicated by the arrows above the spectra.

In this paper, TR^3 spectra were obtained with two probe excitation wavelengths in order to characterize the T_1 state of BP, the DPK radical, and also the long-lived LAT intermediate assigned explicitly to a 2-[4-(hydroxylphenylmethylene)cyclohexa-2,5-dienyl]propan-2-ol cross-coupling product (referred to hereafter as the *p*-DPK-DMK species in this paper) formed from reaction of the DPK radical and the dimethylketyl (DMK) radical. To our knowledge, this is the first TR^3 characterization of the LAT intermediates and dynamics for its formation in the photoreaction of BP in 2-propanol. TR^3 experiments were first performed in acetonitrile (MeCN) solvent where the hydrogen abstraction reaction to produce the DPK radical does not occur and the long-lived LAT intermediate is not observed. The TR^3 spectra obtained in MeCN solvent enable clear characterization of the spectra associated with the T_1 state of BP and help to clearly distinguish it from other transient species associated with the hydrogen abstraction reaction and subsequent formation of the LAT intermediate in TR^3 experiments performed in the 2-propanol solvent. To help determine the geometries and vibrational frequencies of these transient species and to make assignments to the experimental vibrational bands, density functional theory (DFT) calculations were also done that employed the (U)B3LYP methods with a 6-311G** basis set for all of these species of interest. We briefly discuss the structures and properties of the DPK radical and the *p*-DPK-DMK cross-coupling product intermediates that we observed and identified in our TR^3 and DFT studies.

Results and Discussion

A. Time-Resolved Resonance Raman (TR^3) Spectroscopy of BP in MeCN. Figure 1 displays the absorption spectra of BP in pure MeCN and 2-propanol, and the pump and probe wavelengths used in the TR^3 measurements are indicated by arrows in the figure. Figure 1S in the Supporting Information shows the ns-TR^3 spectra of BP in pure MeCN obtained at various time delays from 0 to 500 ns under open air (a) and O_2 purge (b) conditions, using a 266 nm pump wavelength and a 319.9 nm probe wavelength. The top of Figure 2 presents an expanded view of a TR^3 spectrum selected from the spectra

(5) (a) Miyasaka, H.; Morita, K.; Kamada, K.; Mataga, N. *Bull. Chem. Soc. Jpn.* **1990**, *63*, 131−137. (b) Tamai, N.; Asahi, T.; Masuhara, H. *Chem. Phys. Lett.* **1992**, *198*, 413−418. (c) Ramseier, M.; Senn, P.; Wirz, J. *J. Phys. Chem. A* **2003**, *107*, 3305−3315.

(6) (a) Shah, B. K.; Neckers, D. C. *J. Am. Chem. Soc.* **2004**, *126*, 1830−1835. (b) Shah, B. K.; Rodgers, M. A. J.; Neckers, D. C. *J. Phys. Chem. A* **2004**, *108*, 6087−6089.

(7) (a) Sakamoto, M.; Cai, X.; Hara, M.; Tojo, S.; Fujitsuka, M.; Majita, T. *J. Phys. Chem. A* **2004**, *108*, 8147−8150. (b) Cai, X.; Sakamoto, M.; Fujitsuka, M.; Majima, T. *Chem. Eur. J.* **2005**, *11*, 6471−6477. (c) Sakamoto, M.; Cai, X.; Fujitsuka, M.; Majima, T. *Chem. Eur. J.* **2006**, *12*, 1610−1617.

(8) (a) Pitts, J. N., Jr.; Letsinger, R. L.; Taylor, R. P.; Patterson, J. M.; Recktenwald, G.; Martin, R. B. *J. Am. Chem. Soc.* **1959**, *81*, 1068−1077. (b) Beckett, A.; Porter, G. *Trans. Faraday Soc.* **1963**, *59*, 2038−2050. (c) Backström, H. L. J.; Appelgren, K. L.; Niklasson, R. J. V. *Acta Chem. Scand.* **1965**, *19*, 1555−1560. (d) Schenck, G. O.; Cziesla, M.; Eppinger, K.; Matthias, G.; Pape, M. *Tetrahedron Lett.* **1967**, *3*, 193. (e) Filipescu, N.; Minn, F. L. *J. Am. Chem. Soc.* **1968**, *90*, 1544−1547. (f) Chilton, J.; Guering, L.; Steel, C. *J. Am. Chem. Soc.* **1976**, *98*, 1865−1870. (g) Colman, P.; Dunne, A.; Quinn, M. F. *J. Chem. Soc., Faraday Trans. I* **1976**, *72*, 2605−2609. (h) Rubin, M. B. *Tetrahedron Lett.* **1982**, *23*, 4615−4618. (i) Demeter, A.; László, B.; Bérces, T. *Ber. Bunsenges. Phys. Chem.* **1988**, *92*, 1478−1485. (j) Demeter, A.; Bérces, T. *J. Photochem. Photobiol. A: Chem.* **1989**, *46*, 27−40. (k) Demeter, A.; Bérces, T. *J. Phys. Chem.* **1991**, *95*, 1228−1232. (l) Albini, A.; Bortolus, P.; Fasini, E.; Monti, S.; Negri, F.; Orlandi, G. *J. Chem. Soc., Perkin Trans.* **1993**, *2*, 691−695. (m) Viltres Costa, C.; Grela, M. A.; Churio, M. S. *J. Photochem. Photobiol. A: Chem.* **1996**, *99*, 51−56. (n) Fister, J. C.; Harris, J. M. *Anal. Chem.* **1995**, *67*, 701−709.

(9) (a) Tahara, T.; Hamaguchi, H.; Tasumi, M. *J. Phys. Chem.* **1987**, *91*, 5875−5880. (b) Tahara, T.; Hamaguchi, H.; Tasumi, M. *Chem. Phys. Lett.* **1988**, *152*, 135−139. (c) Tahara, T.; Hamaguchi, H.; Tasumi, M. *J. Phys. Chem.* **1990**, *94*, 170−178. (d) Yabumoto, S.; Sato, S.; Hamaguchi, H. *Chem. Phys. Lett.* **2005**, *416*, 100−103.

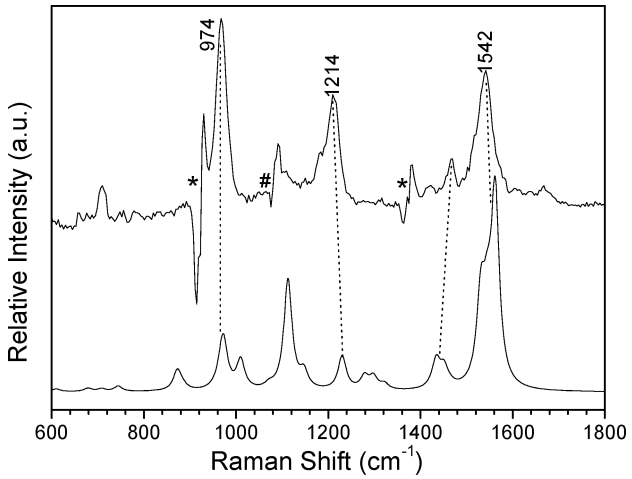

FIGURE 2. Comparison of the experimental resonance Raman spectra (~10 ns time delay) of benzophenone obtained in MeCN (top) with the DFT calculated spectra for the triplet of the BP (bottom). The asterisk (*) marks solvent subtraction artifacts and the pound sign (#) indicates a stray laser line.

displayed in Figure 1S of the Supporting Information. The 266 nm pump wavelength excites the strong $\pi-\pi^*$ transition of BP. The time dependence of the 1542 cm^{-1} Raman band area of the BP intermediate observed in spectra a and b in Figure 1S is shown in Figure 2S of the Supporting Information and was used to follow the kinetics of this species under open air (open squares) and O_2 purge (open circles) conditions. The kinetics in Figure 2S for this BP intermediate can be fit very well by a one-exponential decay function with time constants of about 75 ns for open air and 26 ns under O_2 purge conditions. The significant decrease of the lifetime of the intermediate under O_2 purge conditions indicates the BP intermediate observed is likely triplet in nature and these results are consistent with previous TR^3 results reported by Hamaguchi and co-workers.[9]

To verify the triplet state BP assignment for the intermediate observed in the TR^3 spectra of Figure 1S, DFT calculations were done and these results were compared to the experimental spectra. Figure 2 displays a comparison between the experimental TR^3 spectrum obtained at 10 ns in Figure 1S(a) to the B3LYP/6-311G** DFT calculated normal Raman spectrum of the BP triplet state. Preliminary Raman band assignments for the BP triplet state were made based on the correlation between the experimental and calculated Raman spectra shown in Figure 2 and Table 1S in the Supporting Information lists these tentative vibrational assignments with nominal descriptions of the normal modes. Four major Raman bands, at 974, 1182, 1214, and 1542 cm^{-1}, were observed. Most of the Raman bands seen in the TR^3 spectra of the BP T_1 state are due to vibrations associated with the ring C−C stretch and C−H bend motions. The 1542 cm^{-1} Raman band is mainly due to a ring C−C stretch vibrational mode. The 1214 cm^{-1} Raman band is mostly from a T_1 carbonyl C═O stretching mode that is substantially downshifted (by ~445 cm^{-1} in frequency) compared to the 1659 cm^{-1} band observed for the ground state BP carbonyl stretch band. The 1182 cm^{-1} Raman band is associated with a C−H in-plane bending of the ring vibration motion. The 974 cm^{-1} Raman feature is attributed to the C−C ring deformation mode. These observed frequencies and their assignments agree well with corresponding TR^3 spectra and assignments previously determined by Hamuguchi and co-workers.[9] Figure 2 reveals that the calculated Raman spectrum shows reasonable agreement with the experimental TR^3 spectrum for the BP triplet state in terms of the vibrational frequencies. However, close examination shows differences between the relative intensity patterns of the experimental spectrum and the calculated spectrum in Figure 2. This can be attributed to the experimental spectrum being resonantly enhanced while the calculated spectrum is a non-resonant Raman spectrum.

Figure 3S in the Supporting Information shows a simple diagram of the optimized geometry and selected structural parameters obtained from (U)B3LYP/6-311G** calculations for the BP triplet state. The bond lengths vary substantially on going from the ground state to the triplet state. Comparison of the triplet state structure with that for the ground state reveals that the carbonyl bond is lengthened by about 0.1 Å while the C1−C3 and C1−C9 bonds which connect the carbonyl group and the two phenyl rings are shortened by about 0.057 Å to become about 1.446 and 1.445 Å, respectively, in the triplet state. The frequency of the carbonyl C−O stretch dominated mode is characteristic in reflecting the nature and properties of the triplet states for aromatic carbonyl compounds. For the benzophenoe triplet state, the remarkable downshift (~455 cm^{-1}) of the T_1 carbonyl stretch mode upon going to the corresponding ground state frequency indicates there is a strong weakening of this bond in the triplet state and this is in agreement with the calculated 0.1 Å increase of the C−O bond length on going from the ground state to the triplet state. This also implies that the carbonyl group in the triplet state has a single bond character as compared with the typical double C═O bond in the ground state.

For aromatic carbonyl compounds, the electronic configuration of the T_1 state determines the T_1 state's reactivity toward the hydrogen abstraction reaction with hydrogen donor reagents. Two types of T_1 states, dominated respectively by $n\pi^*$ and $\pi\pi^*$, have been identified to be responsible for the differences in the T_1 photophysical and photochemical behavior.[10] A T_1 with mainly $n\pi^*$ nature exhibits a high efficiency for hydrogen abstraction reaction whereas a triplet state with a $\pi\pi^*$ nature is barely reactive for that type of reaction. Previous TR^3 and TRIR studies found that the frequency of the C−O stretch mode appears in the 1400−1600 cm^{-1} range for a $\pi\pi^*$ dominated triplet state while it is in the 1200−1400 cm^{-1} region for a typical $n\pi^*$ nature triplet state.[11−14] As illustrated above, the C−O stretch frequency for the BP T_1 state is at ~1210 cm^{-1}. This is fully consistent the T_1state of BP having a $n\pi^*$ dominated

(10) (a) Wagner, P. J.; Puchalski, *J. Am. Chem. Soc.* **1980**, *102*, 6177−6178. (b) Wagner, P. J.; Siebert, E. J. *J. Am. Chem. Soc.* **1981**, *103*, 7329−7335. (c) Wagner, P. J.; Truman, R. J.; Puchalski, A. E.; Wake, R. *J. Am. Chem. Soc.* **1986**, *108*, 7727−7738.

(11) Webb, S. P.; Yeh, S. W.; Phillips, L. A.; Tolbert, M. A.; Clark, J. H. *J. Am. Chem. Soc.* **1984**, *106*, 7286−7288.

(12) Webb, S. P.; Phillips, L. A.; Yeh, S. W.; Tolbert, L. M.; Clark, J. H. *J. Phys. Chem.* **1986**, *90*, 5154−5164.

(13) (a) Schwartz, B. J.; Peteanu, L. A.; Harris, C. B. *J. Phys. Chem.* **1992**, *96*, 3591−3598. (b) Toscano, J. P. *Adv. Photochem.* **2001**, *26*, 41−91. (c) Toscano, J. P. In *Reviews of Reactive Intermediate Chemistry*; Platz, M. S., Moss, R. A., Jones, M., Jr., Eds.; John Wiley and Sons, Inc.: Hoboken, NJ, 2007; pp 183−206.

(14) (a) Ma, C.; Chan, W. S.; Kwok, W. M.; Zuo, P.; Phillips, D. L. *J. Phys. Chem. B* **2004**, *108*, 9264−9276. (b) Ma, C.; Zuo, P.; Kwok, W. M.; Chan, W. S.; Kan, J. T. W.; Toy, P. H.; Phillips, D. L. *J. Org. Chem.* **2004**, *69*, 6641−6657. (c) Chan, W. S.; Ma, C.; Kwok, W. M.; Phillips, D. L. *J. Phys. Chem. A* **2005**, *109*, 3454−3469. (d) Zuo, P.; Ma, C.; Kwok, W. M.; Chan, W. S.; Phillips, D. L. *J. Org. Chem.* **2005**, *70*, 8661−8675. (e) Ma, C.; Kwok, W. M.; Chan, W. S.; Zuo, P.; Kan, J. T. W.; Toy, P. H.; Phillips, D. L. *J. Am. Chem. Soc.* **2005**, *127*, 1463−1427. (f) Ma, C.; Kwok, W. M.; Chan, W. S.; Du, Y.; Kan, J. T. W.; Toy, P. H.; Phillips, D. L. *J. Am. Chem. Soc.* **2006**, *128*, 2558−2570.

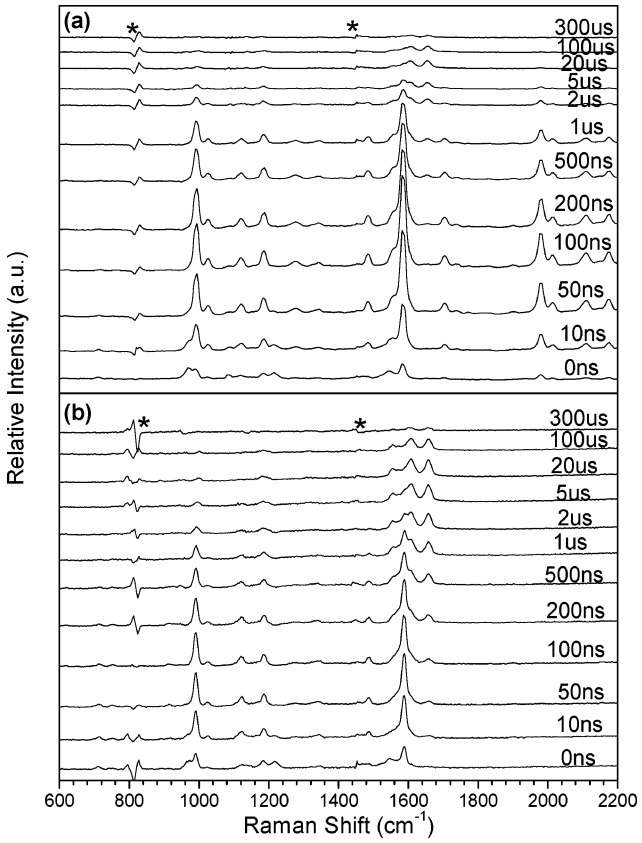

FIGURE 3. Ns-TR^3 spectra observed after 266 nm photolysis of BP in 2-propanol and obtained with 319.9 (a) and 354.7 nm (b) probe wavelengths at various delay times that are indicated next to the spectra. The asterisks (∗) mark solvent subtraction artifacts.

configuration and being capable of abstracting a hydrogen atom from a variety of substrate molecules including hydrocarbons, alcohols, and amines with high efficiency. In the subsequent sections of this paper, the focus will be on the reaction of the BP T_1 state with 2-propanol (a strong hydrogen donor solvent).

B. TR^3 Observation of the Diphenylketyl (DPK) Radical and a Long Lifetime Coupling Complex (LAT) Intermediate in 2-Propanol. Figure 3 presents ns-TR^3 spectra obtained after 266 nm photolysis of BP in 2-propanol and with 319.9 (a) and 354.7 nm (b) probe wavelengths, respectively, at various delay times that are indicated next to the spectra. When employing these two probe wavelengths, the BP triplet state signal can still be observed at early time delays in the 0−10 ns range as indicated by the similarity of the 0 ns spectra of Figure 3a,b to the BP T_1 spectrum recorded in MeCN (see Figure 2). As noted before, the BP triplet state exhibits nπ* character and will be quenched readily and efficiently to produce the DPK radical via a hydrogen abstraction reaction with hydrogen donor solvents such as 2-propanol. Once the BP triplet state is quenched, a new species is observed in the TR^3 spectra of Figure 3 and this new species is tentatively attributed to the DPK radical based on similar observations by Hamaguchi and co-workers in previous work[9] as well as TR^3 spectra of different ketyl radicals observed by Umapathy and co-workers.[15] From comparison of the spectra in Figure 3a obtained with a 319.9 nm probe wavelength with spectra in Figure 3b obtained with a 354.7 nm probe wavelength, one can observe the same quenching of the BP triplet and the same formation of the DPK radical over the 10 to 30 ns time delay range at both wavelengths.

(15) (a) Balakrishnan, G.; Umapathy, S. *Chem. Phys. Lett.* **1997**, *270*, 557−563. (b) Anandhi, R.; Umapathy, S. *J. Raman Spectrosc.* **2000**, *31*, 331−338. (c) Balakrishnan, G.; Mohandas, P.; Umapathy, S. *J. Phys. Chem. A* **2001**, *105*, 7778−7789. (d) Puranik, M.; Umapathy, S.; Snijders, J. G.; Chandrasekhar, J. *J. Chem. Phys.* **2001**, *115*, 6106−6114.

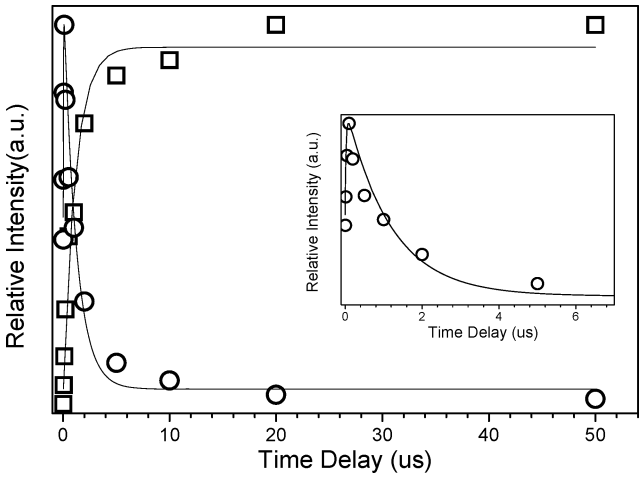

FIGURE 4. Time dependence of the 1585 cm^{-1} Raman band area of DPK (open circles) fit with a two exponential function with ∼27 ns growth time constant and 1170 ns decay time constant (red line). Time dependence of the 1605 cm^{-1} Raman band of the coupling complex (LAT) intermediate *p*-DPK-DMK (open squares) fit with a single-exponential growth function with a time constant of 1150 ± 120 ns (black line). The inset displays the expanded view of 1585 cm^{-1} during the first 7 μs. The data displayed here were derived from the TR^3 spectra shown in Figure 2 (see the text for the more details).

For the 319.9 nm probe wavelength TR^3 spectra, strong signals for the overtone and combination bands of the 992, 1024, 1123, and 1188 cm^{-1} are observed and this implies that the 319.9 nm probe wavelength is significantly in resonance with a strong absorption band of the DPK radical so that the correlated vibrational bands of this species will be strongly resonantly enhanced in the TR^3 spectra obtained at such a probe wavelength. This result is in very good agreement with previous LFP studies showing a characteristic strong DPK radical absorption in the 310−320 nm region.[8j] This is also confirmed by our results from TD-DFT-RPA calculations that found that the BP DPK radical has one strong electronic transition at 322 nm with an oscillator strength of 0.36 (see Table 3S in the Supporting Information). In this sense, the lack of the overtone and combination bands in the 354.7 nm spectra is expected since the 354.7 nm probe wavelength is reasonably far away from the DPK radical absorption maximum. Assignments for the Raman bands observed in the TR^3 spectra for the DPK radical were based on correlation to the predicted Raman spectra from the DFT calculations (see Table 4S in the Supporting Information). Most of the fundamental Raman bands observed for the TR^3 spectra of the DPK radical are due to vibrations associated with the ring C−C stretch and C−H bend motions. For example, the 1024, 1123, and 1188 cm^{-1} vibrational bands have major contributions from ring C−H in-plane bend motions while the 1585 cm^{-1} vibrational band has major contributions from the ring center C−C stretch motions.

The 1585 cm^{-1} Raman features in Figure 3b for the DPK radical were fit with Lorentzian band shapes to obtain the time dependence of this species and the kinetics obtained are displayed in Figure 4 (open circles) with the data points fit by

a two-exponential function with a growth time constant of 27 ns and a decay time constant of 1170 ns.

Examination of the TR^3 spectra in Figure 3 reveals that the decay of the DPK Raman signal (with time constant of 1170 ns) is correlated with the growth of a new set of Raman features due to a new species. This new species has a characteristic 1605 cm^{-1} Raman band that can be used to follow the time-dependent behavior of the new species and a fit to these data in Figure 4 shows that the new species has an exponential growth time constant of ~1150 ns. The time constants for the decay of DPK (1170 ± 120 ns) and the growth of the new species (1150 ± 120 ns) are close to each other and within the uncertainty of the measurements and this indicates that DPK is a precursor for the formation of the new species. For the 319.9 nm probe wavelength TR^3 spectra (Figure 3a), the intensity of the transient Raman signal for this new species is not very large and this implies that the 319.9 nm probe wavelength is not fully resonant with the absorption band of this new species. To confirm this hypothesis and also to obtain stronger structural and kinetic information for this new species, we obtained additional TR^3 spectra using a 354.7 nm probe wavelength and these spectra are displayed in Figure 3b. Examination of Figure 3b shows that the 354.7 nm probe wavelength TR^3 spectra display a stronger TR^3 signal for the new species spectra relative to the DPK spectra and this suggests the 354.7 nm probe wavelength is more on resonance with the absorption of the new species than the 319.9 nm probe wavelength used to obtain the TR^3 spectra in Figure 3a.

Since the DPK radical TR^3 signal decay corresponds to the growth of the new species TR^3 signal in the spectra of Figure 3, it is likely that the DPK radical is reacting with another species to quickly produce the new species observed in the TR^3 spectra. Since the hydrogen abstraction reaction of the triplet benzophenone with the 2-propanol that forms the DPK radical also produces a dimethylketyl (DMK) radical, a cross-coupling reaction of the DPK radical with the DMK radical to form cross-coupling products such as 2-[4-(hydroxylphenylmethylene)-cyclohexa-2,5-dienyl]propan-2-ol (*p*-DPK-DMK) and/or a 2-[6-(hydroxylphenylmethylene)cyclohexa-2,4-dienyl]propan-2-ol (*o*-DPK-DMK) could be likely possibilities. B3LYP/6-311G** DFT calculations were performed to determine the optimized structures of the *p*-DPK-DMK and *o*-DPK-DMK cross-coupling products (see Figure 5 for a schematic diagram of the optimized geometry structures). We note that a previous study by Demeter and Bérces[8j] using transient absorption experiments and other indirect evidence from the absorption spectra of 1-phenylbutadiene and 1-phenylhexatriene tentatively assigned the LAT intermediates to the *p*-DPK-DMK species having a λ_{max} at about 317 nm and ϵ_{max} of about 28 000 L mol^{-1} cm^{-1} and the *o*-DPK-DMK species having a λ_{max} at about 358 nm and ϵ_{max} of about 50 000 L mol^{-1} cm^{-1}. Our present results from TD-DFT (B3LYP/6-311G**) RPA calculations shown in Table 3S in the Supporting Information show that at wavelengths longer than 300 nm the *p*-DPK-DMK species has only one strong electronic transition at about 352 nm with an oscillator strength of 0.48 while the *o*-DPK-DMK species has two strong electronic transitions at 466 and 320 nm with oscillator strengths of 0.13 and 0.12, respectively. These results lead to a different assignment of the transient absorption bands observed for the LAT intermediates in previous studies so that the LAT transient absorptions with maxima at about 358 and 317 nm should be assigned to the *p*-DPK-DMK and the *o*-DPK-DMK species, respectively.

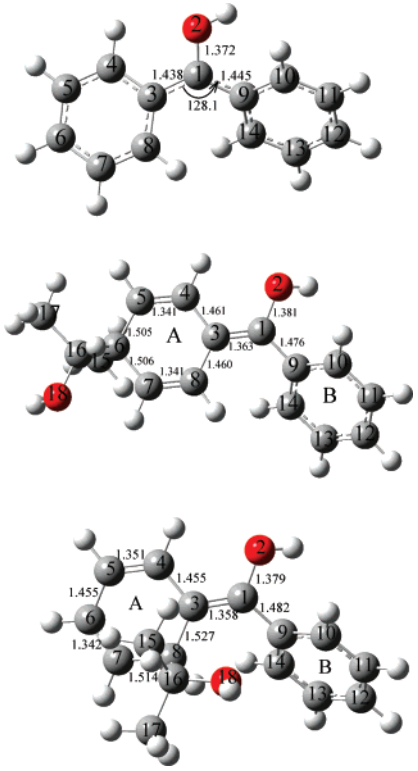

FIGURE 5. Optimized structure of DPK (top) and the 2-[4-(hydroxylphenylmethylene)cyclohexa-2,5-dienyl]propan-2-ol (*p*-DPK-DMK) and 2-[6-(hydroxylphenylmethylene)cyclohexa-2,4-dienyl]propan-2-ol (*o*-DPK-DMK) cross-coupling products (middle and bottom, respectively) calculated from the B3LYP/6-311G** DFT calculations. Selected bond lengths (in Å) and bond angles (in deg) are labeled.

Figure 6 displays a comparison between the experimental TR^3 spectra obtained at 50 ns and 50 μs in Figure 3 to the B3LYP/6-311G** DFT calculated normal Raman spectra for the DPK radical (Figure 6a), *p*-DPK-DMK and *o*-DPK-DMK (spectra e and f in Figure 6, respectively) cross-coupling products, and the two cross-coupling spectra with equal contributions (Figure 6g). Inspection of Figure 6 reveals that the calculated normal Raman spectra for the DPK radical (Figure 6a) and the *p*-DPK-DMK cross-coupling product (Figure 6e) exhibit reasonable agreement with the experimental TR^3 spectra obtained at 50 ns (Figure 6, b and c) and 50 μs (Figure 6d), respectively. The experimental and calculated spectra in Figure 6 show moderate differences in their relative Raman intensity pattern and this can be accounted for by the experimental spectra being resonantly enhanced while the calculated spectra are nonresonant Raman spectra. Preliminary Raman band assignments for the DPK radical and the *p*-DPK-DMK cross-coupling product were made based on the correlation between the experimental and calculated Raman spectra shown in Figure 6. Table 2 lists the tentative vibrational assignments with nominal descriptions of the normal modes. Inspection of Figure 6 and Table 4S (Supporting Information) reveals the calculated vibrational frequencies for the *p*-DPK-DMK species agree significantly better with the experimentally observed TR^3 Raman bands for the LAT species than the frequencies calculated for the *o*-DPK-DMK species. For example, the calculated vibrational frequencies for the *p*-DPK-DMK species are within about 8.4 cm^{-1} on average for the nine experimental TR^3 Raman band frequencies

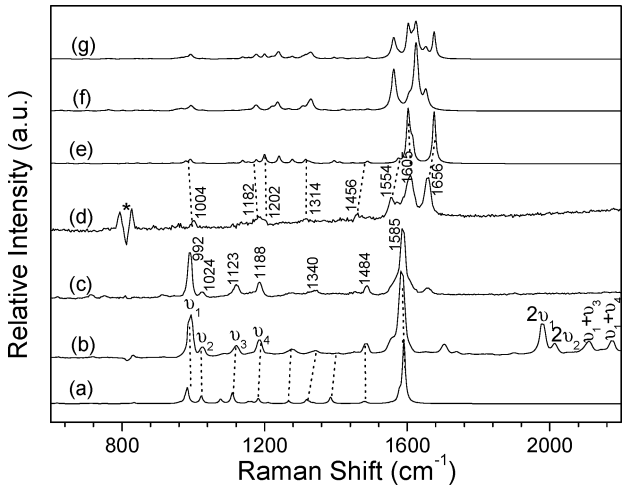

FIGURE 6. Comparison of the experimental TR^3 spectra obtained after photolysis of BP in 2-propanaol solvent at a 50 ns delay time by using 319.9 (b) and 354.7 nm (c) probe wavelengths and at a 50 μs delay time by using a 354.7 nm probe wavelength (d) to the Raman spectra obtained from B3LYP/6-311G** DFT calculations for the DPK radical (a), the *o*-DPK-DMK species (f), the *p*-DPK-DMK species (e), and both the *o*-DPK-DMK and *p*-DPK-DMK with equal contributions (g). Dotted lines display the correlation between the experimental and calculated Raman bands (see the text for more details).

for the LAT species while the *o*-DPK-DMK are within about 19 cm^{-1} on average to the experimental values. It is also useful to note that the predicted excited state energies and oscillator strengths from TD-DFT (B3LYP/6-311G**) RPA calculations for *p*-DPK-DMK species shown in Table 3S (Supporting Information) are consistent with the experimental TR^3 spectra shown in Figure 3. For example, the calculations in Table 3S (Supporting Information) predict a very strong transition at 352 nm with oscillator strength of 0.48 and a weaker transition at 321 nm with an oscillator strength of 0.012 and these correlate well with the long-lived LAT species observed in the TR^3 spectra of Figure 3 being strong in the 354.7 nm probe wavelength and noticeably weaker for the 319.9 probe wavelength spectra. It is also important to note that the predicted excited state energies and oscillator strengths from TD-DFT (B3LYP/6-311G**) RPA calculations for *o*-DPK-DMK species shown in Table 3S (Supporting Information) are not consistent with the experimental TR^3 spectra shown in Figure 3. For example, the calculations indicate that *o*-DPK-DMK has only weak transitions at 353 and 343 nm and strong transitions at 466 and 320 nm between 300 and 500 nm and this disagrees with the strong TR^3 spectra observed for the LAT intermediate at 354.7 nm and a weaker spectrum at the 319.9 nm wavelength in Figure 3. The good agreement between the long time experimental TR^3 spectra and their wavelength-dependent behavior with the DFT calculated normal Raman spectra (see Figure 6 and Table 4S (Supporting Information)) and the DFT calculated excited-state transition energies and oscillator strengths (see Table 3S in the Supporting Information) for the *p*-DPK-DMK species provide a clear assignment of this species to the long-lived LAT species observed in the TR^3 spectra of Figure 3. Our present TR^3 results show the formation of the *p*-DPK-DMK cross-coupling product from the reaction of the diphenylketyl radical (DPK) and the dimethylketyl radical (DMK) directly correlates with the decay of the DPK species and that this occurs with a time constant of about 1150 ns under the conditions employed in our experiments.

C. Discussion of the Structures and Properties of the Diphenylketyl (DPK) Radical and the 2-[4-(Hydroxylphenylmethylene)cyclohexa-2,5-dienyl]propan-2-ol (*p*-DPK-DMK) Species Assigned to the Long-Lived LAT Intermediate. The structure and properties of the DPK radical and the *p*-DPK-DMK species assigned to the long-lived LAT intermediate are significantly different from one another. Figure 5 presents some selected bond lengths and bond angles for DPK and the *p*-DPK-DMK species and Table 2S in the Supporting Information gives a more comprehensive list of the structural parameters. Inspection of the structures shown in Figure 5 reveals that when DPK reacts with DMK to produce the *p*-DPK-DMK species, the structure of the ring A part that connects with DMK significantly changes its structure. For example, the C1−C3, C4−C5, and C7−C8 bonds become noticeably shorter with lengths around 1.34 Å and have typical double bond character. Thus, the cross-coupling reaction between DPK and DMK results in the ring A having a cyclohexadienyl character with an enol moiety attached to this ring in the *p*-DPK-DMK species (see Figure 5). It is also important to note that this increase of cyclohexadienyl character in ring A is accompanied by noticeable changes in the enol moiety, the bonds connecting ring A and ring B, and the relative orientation between the two rings. For example, the C1−C3 and C1−C9 bonds connecting the two rings go from 1.438 and 1.445 Å in DPK to become 1.363 and 1.476 Å, respectively, in *p*-DPK-DMK. This indicates that the C1−C3 bond gains double bond character leading to the enol formation while the C1−C9 bond gains more single bond character and these changes appear to be an extension of the cyclohexadienyl conjugation system. It is interesting to note that the ring A C4−C5 and C7−C8 bonds have somewhat stronger double bond (bond lengths of 1.341 Å) character than the enol C1−C3 bond (1.363 Å). The formation of the cyclohexadienyl/enol character in *p*-DPK-DMK also results in the O2−C1−C3−C4 and O2−C1−C9−C10 dihedral angles changing noticeably from 18.3° and 25.1° in DPK to 7.4° and 39.1° in *p*-DPK-DMK and this may suggest some moderate interaction of the cyclohexadienyl ring A/enol part of the system with the phenyl ring B part of *p*-DPK-DMK.

It is clear that the structure of *p*-DPK-DMK is significantly different from that of DPK and one would expect their chemical reactivities to be substantially different as well. Our TR^3 results clearly observe that under our experimental conditions the main decay pathway of DPK is its cross-coupling reaction with DMK (with a time constant of about 1170 ns) to produce the long-lived *p*-DPK-DMK intermediate. This is consistent with the transient absorption studies of Demeter and Bérces[8j] and Albini and Bortolis and co-workers[8l] that showed the long-lived LAT intermediate appeared to be formed from the reaction of DPK and DMK. Since the *p*-DPK-DMK intermediate has a substantially longer lifetime, it appears to be a less reactive species than DPK. We found that the main final products from our experiments were benzopinacol and acetone and this is consistent with the large body of photochemistry results reported previously in the literature.[1,2,8] Several previous studies[8e,j] noted that the decomposition of the LAT intermediate with an absorption maximum at about 358 nm (that we have shown here is predominantly due to the *p*-DPK-DMK species) depends on the concentration of BP and this suggests that the LAT intermediate may be reacting with BP to produce the final products (e.g., possibly a reaction like *p*-DPK-DMK + BP → benzopinacol + acetone). Further work to more explicitly

characterize the decay of the *p*-DPK-DMK species and the formation of its decay products may be attractive for future investigation.

A TR^3 spectrum that had similar amounts of *o*- and *p*-DPK-DMK present would probably look similar to the predicted Raman spectrum shown at the top of Figure 6 that shows some new Raman bands specific to the *o*-DPK-DMK species that are not seen in the 354.7 nm TR^3 spectrum or the calculated *p*-DPK-DMK Raman spectrum (Figure 6d,e). Our 319.9 and 354.7 nm TR^3 spectra on the tens to hundreds of microseconds time scale show that essentially the same *p*-DPK-DMK species was observed at both wavelengths. If appreciable *o*-DPK-DMK were present, according to our TD-DFT-RPA calculation results, we would expect that new Raman bands specific to this isomer would appear in the 319.9 nm TR^3 spectra where *o*-DPK-DMK is predicted to have a strong absorption at about 320 nm with an oscillator strength of 0.12 while the *p*-DPK-DMK has a much weaker transition at 321 nm with an oscillator strength of 0.012 and is somewhat off-resonance with the nearby stronger transition at 352 nm with an oscillator strength of 0.48. However, we did not observe any obvious *o*-DPK-DMK features in the TR^3 spectra. This could be due to a combination of several factors. The B3LYP/6-311G** DFT calculations found that *p*-DPK-DMK is about 6.5 kcal/mol more stable than *o*-DPK-DMK and this indicates there is probably noticeable steric interaction between the isopropyl moiety and ring A of the DPK-DMK system. A steric interaction similar to this may make it more difficult for the DMK radical to react at the ortho site compared to the para site of the DPK radical and kinetically lead to production of more *p*-DPK-DMK relative to *o*-DPK-DMK. In addition, the TR^3 experiments would be noticeably more sensitive to detection of *p*-DPK-DMK at the 354.7 nm wavelength that is resonant with its strong transition predicted at 352 nm with an oscillator strength of 0.48 compared to *o*-DPK-DMK at the 319.9 nm wavelength that is resonant with its strong transition predicted at 320 nm with an oscillator strength of 0.12. These factors would make it more difficult to observe a modest amount of *o*-DPK-DMK intermediate and it is not clear just how much of this isomer is present.

The most intense Raman bands observed for the TR^3 spectra of the *p*-DPK-DMK species assigned to the long-lived LAT intermediate are due to vibrations associated with the C−C stretching motions of the phenyl rings and the enol moiety (see Table 4S in the Supporting Information). For example, the 1656 cm^{-1} Raman mode has motions predominantly in the C1−C3, C4−C5, and C7−C8 stretching motions, the 1605 cm^{-1} Raman mode has contributions mainly from the C4−C5, C7−C8 ring A stretching motions accompanied by a moderate amount of the ring B C−C stretching motions, and the 1554 cm^{-1} Raman mode has contributions mainly from the C−C stretching motions on ring B accompanied by the C1−C3 bond of the enol moiety. Figure 7 presents a diagram depicting the electron density for the HOMO and LUMO associated for the strong 352 nm absorption transition predicted from the TD-DFT calculations (see Table 1).

Examination of Figure 7 reveals that there is a substantial change in the electron density in the ring A and enol parts accompanied by some changes in the ring B part of the *p*-DPK-DMK species as the HOMO goes to the LUMO for the 352 nm transition. This is consistent with the strong intensity in the TR^3 Raman bands associated mainly with C−C stretch motions of the ring A, enol and ring B parts of the molecule associated with the vibrational modes in the 1500−1700 cm^{-1} region. This provides further support for the assignment of the LAT species characterized here to be from the *p*-DPK-DMK species.

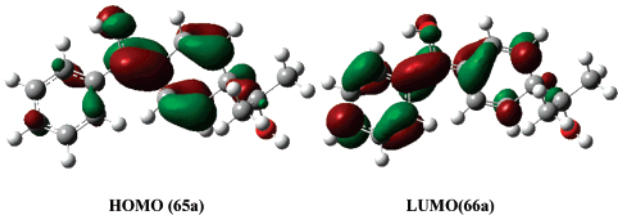

FIGURE 7. Simple schematic diagrams depicting the electron density for the HOMO and LUMO associated with the strong 352 nm absorption transition predicted from the TD-DFT calculations for the *p*-DPK-DMK species (see Figure 5, as well as Table 3S in the Supporting Information).

It is interesting to note that there is not a noticeable fast component for the formation of the *p*-DPK-DMK species from the initially formed DPK and DMK species from the triplet BP hydrogen abstraction reaction with 2-propanol that was observed to occur within tens of nanoseconds time scale. This suggests there is no substantial geminate recombination of the DPK and DMK radicals and they are initially produced with a configuration relative to one another that is unfavorable for the coupling reaction to occur immediately by geminate recombination and they likely escape the solvent cage. If geminate recombination (and/or reaction) between the two radicals in the geminate pair occurs then this process is expected to take place in a very short time (like a few picoseconds to a few tens of picoseconds).[16] This is clearly not the case observed here where a significant amount of time is apparently needed to reach favorable conditions for the DPK and DMK radicals to undergo a coupling reaction to produce the *p*-DPK-DMK intermediate that is observed to occur with a time constant of about 1170 ns and whose growth correlates to the decay of DPK radical in the TR^3 experiments (see Figures 3 and 4). This is likely a bimolecular coupling reaction by two free radicals with a rate constant near the diffusion limit that may be expected for a radical−radical reaction.[17] We note that similar metastable coupling species (termed "light absorbing transients") are also known in the photoreduction of other species.[17] For example, the mutual recombination of ketyl radicals produced by hydrogen abstraction was suggested to be the main reaction mechanism responsible for an acid release in phenacyl ester photoreduction in the presence of a low concentration of the H-atom donor.[17a] In addition, relatively long-lived metastable coupling intermediates were also observed after photolysis of phenacyl or pyridacyl esters in neat 2-propanol.[17b]

The half-life equation for the second-order reaction dependent on one second-order reactant (DPK in our experiment) is $t_{1/2} = 1/k[\mathrm{DPK}]_0$, where $t_{1/2}$ is the half-life time of DPK species, k is the bimolecular rate constant for the DPK-DMK species, and $[\mathrm{DPK}]_0$ is the initial concentration of the DPK species. To obtain the value of $[\mathrm{DPK}]_0$, we estimated the photoalternation parameter F according to the following formula $F = (2303E\epsilon\varphi)/(\pi r^2 N_A)$, where F is the fraction of molecules photolyzed by a

(16) (a) Hirata, Y.; Ohta, T.; Mataga, N. *J. Phys. Chem.* **1992**, *96*, 1517−1520. (b) Bultmann, T.; Ernsting, N. P. *J. Phys. Chem.* **1996**, *100*, 19417−19424. (c) Lochschmidt, A.; Eilers-Konig, N.; Heineking, N.; Ernsting, N. P. *J. Phys. Chem. A.* **1999**, *103*, 1776−1784.

(17) (a) Banerjee, A.; Falvey, D. E. *J. Am. Chem. Soc.* **1998**, *120*, 2965−2966. (b) Literak, J.; Dostalova, A.; Klan, P. *J. Org. Chem.* **2006**, *71*, 713−723.

single pulse with energy E (photons), ϵ is the molar extinction coefficient (M^{-1} cm^{-1}), φ is the photochemical quantum yield, and r is the radius of the focused laser beam (cm).[18] F was estimated to be 0.70 in our experiments for 266 nm pump pulse (see the Supporting Information for details of the estimate). Since the BP T_1 state is produced with a large yield close to unity and the reaction pathway from BP T_1 state to the DPK species is the main pathway in 2-propanol solvent, we estimate the value of $[DPK]_0$ to be about 2.1×10^{-3} M. The bimolecular rate constant for the DPK-DMK species in our experiment was estimated to be about 4×10^8 M^{-1} s^{-1} (using $k = 1/t_{1/2}[DPK]_0 = 1/[(1170 \times 10^{-9}\ s)(2.1 \times 10^{-3}\ M)]$). This value is in good agreement with the results of Viltres Costa and co-workers,[8m] who obtained a bimolecular rate constant of $3.6 \pm 0.4 \times 10^8$ M^{-1} s^{-1} for formation of the DPK-DMK species from transient absorption measurements, and this rate constant is smaller than the diffusion-limited rate constant of about 10^9 M^{-1} s^{-1}. This indicates our present TR^3 results are consistent with previous transient absorption experiments and the DPK species undergoes a second-order bimolecular reaction to form the DPK-DMK species.

We note that the concentration of O_2 is low compared to that of the 2-propanol solvent and the 2-propanaol solvent appears to quench the BP T_1 state noticeably faster (27 ns) than O_2 quenching in acetonitrile solvent (75 ns) under similar ambient conditions. This and our observation that the bimolecular rate constant estimated from the TR^3 experiments (about 4×10^8 M^{-1} s^{-1}) is in good agreement with that measured by transient absorption experiments[8m] for degassed samples ($(3.6 \pm 0.4) \times 10^8$ M^{-1} s^{-1}) suggest that ambient O_2 is not significantly quenching the BP T_1 state in 2-propanol under present conditions. The amount of water impurity in the HPLC grade 2-propanol was 0.05% and this is somewhat larger than the 0.02% water impurity in HPLC grade acetonitrile. We obtained TR^3 spectra after photolysis of BP in an acetonitrile solution to which 0.1% water was added (see Figure 4S in the Supporting Information) and these spectra were essentially the same as those obtained in acetonitrile (see Figure 1S in the Supporting Information) and indicate the water impurity is not responsible for the LAT species.

Conclusions

A nanosecond time-resolved resonance Raman (ns-TR^3) spectroscopic investigation of the T_1 state BP reaction with a 2-propanol solvent and subsequent reactions was described. The TR^3 spectra observed the BP T_1 state ($n\pi^*$) hydrogen-abstraction reaction with 2-propanol occurred on the tens of nanoseconds time scale to produce a DPK radical and an associated DMK radical and recombination of these two radical species via a cross-coupling reaction took place with a time constant of about 1170 ns to produce a LAT intermediate under the reaction conditions employed in our study (3 mM BP in 2-propanol solvent). Comparison of the TR^3 spectra to results from density functional theory calculations were used to identify the LAT intermediate as the 2-[4-(hydroxylphenylmethylene)cyclohexa-2,5-dienyl]propan-2-ol species (*p*-DPK-DMK). This *p*-DPK-DMK intermediate was found to have substantial cyclohexadienyl character in one phenyl ring with an enol moiety attached to this ring. The structure and properties of *p*-DPK-DMK were discussed and compared to those of the DPK radical.

Experimental and Computational Methods

The BP sample used in the TR^3 experiments was commercially obtained from Acros (with >99% purity) and was used as received. Spectroscopic grade acetonitrile (denoted MeCN hereafter) and 2-propanol were used as solvents for the experiments presented in this work. Sample solutions of ~3 mM concentration in pure MeCN and 2-propanol were employed in the TR^3 experiments.

The ns-TR^3 measurements were done using an experimental apparatus and methods described previously.[19] A pump wavelength of 266 nm generated from the fourth harmonic of a Spectra Physics LAB-170-10 Nd:YAG Q-switched laser was employed in the ns-TR^3 experiments. The third anti-Stokes hydrogen Raman shifted laser line pumped by the second harmonic (532.0 nm) was used to produce the 319.9 nm probe wavelength and the third harmonic from the Nd:YAG laser (Spectra Physics GCR-150-10) provided the 354.7 nm probe wavelength used in the ns-TR^3 experiments. The time delay between the pump and probe laser beams was controlled electronically by a pulse delay generator and was monitored by a photodiode and a 500 MHz oscilloscope. The time resolution of the experiments was approximately 10 ns. A near collinear geometry was employed to focus the pump and probe beam onto a flowing liquid stream of sample and the Raman scattering was collected in a backscattering configuration. The Raman signal was detected by a liquid nitrogen cooled CCD detector and acquired by the CCD for 30−60 s before being read out to an interfaced PC computer. Approximately 10 to 20 these readouts were accumulated to get a resonance Raman spectrum. The spectra presented in this work were obtained from subtraction of an appropriately scaled probe-before-pump spectrum from the corresponding pump−probe spectrum. The Raman bands of the acetonitrile solvent were used to calibrate the TR^3 spectra with an estimated accuracy of ± 5 cm^{-1} in absolute frequency. A Lorentzian function was used to integrate the relevant Raman bands in the TR^3 spectra in order to determine their areas and to extract the decay and growth dynamics of the species observed in the experiments.

The optimized geometry, vibrational modes, and vibrational frequencies for the ground state BP, the T_1 state BP, the DPK radical, the *p*-DPK-DMK cross-coupling product intermediate, as well as its ortho isomer *o*-DPK-DMK were obtained from the (U)-B3LYP/6-311G** DFT calculations. No imaginary frequency modes were observed at any of the optimized structures shown here. A Lorentzian function with a 15 cm^{-1} bandwidth was used in conjunction with the calculated Raman vibrational frequencies and their relative intensities to obtain the B3LYP/6-311G** computed Raman spectra to compare with the corresponding experimental TR^3 spectra. TD-DFT-RPA calculations were also done for the species of interest to find the electronic transition energies and their oscillator strengths to compare with the TR^3 results and literature

(18) (a) Mathies, R. A. In *Chemical and Biochemical Applications of Lasers*; Moore, B. B., Ed.; Academic Press: New York, 1979; pp 55−99. (b) Myers, A. B. *Chem. Rev.* **1996**, *96*, 911−926. (c) Phillips, D. L.; Kwok, W. M.; Ma, C. In *Reviews of Reactive Intermediate Chemistry*; Platz, M. S., Moss, R. A., Jones, M., Jr., Eds.; John Wiley and Sons, Inc.: Hoboken, NJ, 2007; pp 123−182.

(19) (a) Zhu, P.; Ong, S. Y.; Chan, P. Y.; Leung, K. H.; Phillips, D. L. *J. Am. Chem. Soc.* **2001**, *123*, 2645−2649. (b) Li, Y.-L.; Leung, K. H.; Phillips, D. L. *J. Phys. Chem. A* **2001**, *105*, 10621−10625. (c) Zhu, P.; Ong, S. Y.; Chan, P. Y.; Poon, Y. F.; Leung, K. H.; Phillips, D. L. *Chem. Eur. J.* **2001**, *7*, 4928−4936. (d) Chan, P. Y.; Ong, S. Y.; Zhu, P.; Leung, K. H.; Phillips, D. L. *J. Org. Chem.* **2003**, *68*, 5265−5273. (e) Chan, P. Y.; Ong, S. Y.; Zhu, P.; Zhao, C.; Phillips, D. L. *J. Phys. Chem. A* **2003**, *107*, 8067−8074. (f) Chan, P. Y.; Kwok, W. M.; Lam, S. K.; Chiu, P.; Phillips, D. L. *J. Am. Chem. Soc.* **2005**, *127*, 8246−8247. (g) Xue, J.; Guo, Z.; Chan, P. Y.; Chu, L. M.; But, T. Y. S.; Phillips, D. L. *J. Phys. Chem. A* **2007**, *111*, 1441−1451.

transient absorption experimental results where available. All of the calculations were done with the Gaussian 03 program suite.[20]

Acknowledgment. This research has been supported by grants from the Research Grants Council of Hong Kong (HKU7040/06P), the award of a Croucher Foundation Senior Research Fellowship (2006−07) from the Croucher Foundation, and an Outstanding Researcher Award (2006) from the University of Hong Kong to D.L.P.

Supporting Information Available: Figure 1S shows ns-TR^3 spectra of BP in pure MeCN obtained under open air and O_2 purge condition with a 266 nm pump wavelength and a 319.9 nm probe wavelength at various time delays; Figure 2S shows the time dependence of the 1542 cm^{-1} Raman band area obtained in Figure 1S under the open air and oxygen purge conditions; Figure 3S shows the optimized structures of the BP ground state and excited triplet state calculated from B3LYP/6-311G** DFT calculations; Figure 4S shows the TR^3 spectra obtained in acetonitrile solvent with 0.1% water added to the solution; the calculation to estimate the photoalternation parameter F is given; Table 1S shows Raman frequencies and assignments for the ground state and triplet states of BP; Table 2S lists the selected bond lengths and bond angles for DPK and the *p*-DPK-DMK species; Table 3S shows excited state energies and oscillator strengths from TD-DFT (B3LYP/6-311G**) RPA calculations for the diphenylketyl radical and the coupling complex (LAT) intermediate assigned to *p*-DPK-DMK and *o*-DPK-DMK; Table 4S shows excited state energies and oscillator strengths from TD-DFT (B3LYP/6-311G**) RPA calculations for the DPK radical, the coupling complex (LAT) intermediate assigned to *p*-DPK-DMK, and *o*-DPK-DMK; and Cartesian coordinates, total energies, and vibrational zero-point energies for the optimized geometry from the B3LYP/6-311G** calculations for the ground state BP, T_1 triplet BP, DPK radical, and the *p*-DPK-DMK and *o*-DPK-DMK cross-coupling products are given. This material is available free of charge via the Internet at http://pubs.acs.org.

JO070958D

(20) Frisch, M. J.; Trucks, G. W.; Schlegel, H. B.; Scuseria, G. E.; Robb, M. A.; Cheeseman, J. R.; Zakrzewski, V. G.; Montgomery, J. A., Jr.; Stratmann, R. E.; Burant, J. C.; Dapprich, S.; Millam, J. M.; Daniels, A. D.; Kudin, K. N.; Strain, M. C.; Farkas, O.; Tomasi, J.; Barone, V.; Cossi, M.; Cammi, R.; Mennucci, B.; Pomelli, C.; Adamo, C.; Clifford, S.; Ochterski, J.; Petersson, G. A.; Ayala, P. Y.; Cui, Q.; Morokuma, K.; Malick, D. K.; Rabuck, A. D.; Raghavachari, K.; Foresman, J. B.; Cioslowski, J.; Ortiz, J. V.; Baboul, A. G.; Stefanov, B. B.; Liu, G.; Liashenko, A.; Piskorz, P.; Komaromi, I.; Gomperts, R.; Martin, R. L.; Fox, D. J.; Keith, T.; Al-Laham, M. A.; Peng, C. Y.; Nanayakkara, A.; Gonzalez, C.; Challacombe, M.; Gill, P. M. W.; Johnson, B.; Chen, W.; Wong, M. W.; Andres, J. L.; Gonzalez, C.; Head-Gordon, M.; Replogle, E. S.; Pople, J. A. *Gaussian 98*, revision A.7 and *Gaussian 03*, revision B.05; Gaussian Inc.: Pittsburgh, PA, 1998; 2003.